ELSEVIER

Marine Geology 215 (2005) 45–57

MARINE GEOLOGY
INTERNATIONAL JOURNAL OF MARINE GEOLOGY, GEOCHEMISTRY AND GEOPHYSICS

www.elsevier.com/locate/margeo

The Grand Banks landslide-generated tsunami of November 18, 1929: preliminary analysis and numerical modeling

I.V. Fine[a,b], A.B. Rabinovich[b,c], B.D. Bornhold[d], R.E. Thomson[b,*], E.A. Kulikov[b,c]

[a]*Heat and Mass Transfer Institute, Minsk, Belarus*
[b]*Institute of Ocean Sciences, Sidney, BC, Canada*
[c]*P.P.Shirshov Institute of Oceanology, Moscow, Russia*
[d]*School of Earth and Ocean Sciences, University of Victoria, BC, Canada*

Accepted 8 November 2004

Abstract

On November 18, 1929, a M=7.2 earthquake occurred at the southern edge of the Grand Banks, 280 km south of Newfoundland. The earthquake triggered a large submarine slope failure (200 km^3), which was transformed into a turbidity current carrying mud and sand eastward up to 1000 km at estimated speeds of about 60–100 km/h, breaking 12 telegraph cables. The tsunami generated by this failure killed 28 people, making it the most catastrophic tsunami in Canadian history. Tsunami waves also were observed along other parts of the Atlantic coast of Canada and the United States. Waves crossing the Atlantic were recorded on the coasts of Portugal and the Azores Islands. Tsunami waves had amplitudes of 3–8 m and runup of up to 13 m along the coast of the Burin Peninsula (Newfoundland). To simulate the slide-generated tsunami from this event, our initial analysis uses a shallow-water model; the slide was assumed to be a viscous, incompressible fluid layer; water was inviscid and incompressible. The preliminary results of the numerical modeling are encouraging, with computed and observed tsunami arrival times in reasonable agreement.

Keywords: tsunami; submarine landslide; 1929 Grand Banks earthquake; numerical modeling

1. Introduction

At 20:32 UTC on November 18, 1929, a magnitude M=7.2 earthquake occurred at an estimated depth of 20 km beneath the sea floor at the southern edge of the Grand Banks (mouth of the Laurentian Channel, Northwest Atlantic), about 280 km south of Newfoundland (Murty, 1977; Piper et al., 1988; Evans, 2001; Clague et al., 2003). The epicenter of the

* Corresponding author.
E-mail addresses: fine@itmo.by (I.V. Fine), RabinovichA@pac.dfo-mpo.gc.ca (A.B. Rabinovich), brian@coastalandoceans.com (B.D. Bornhold), ThomsonR@pac.dfo-mpo.gc.ca (R.E. Thomson), kulikov@korolev.net.ru (E.A. Kulikov).

0025-3227/$ - see front matter © 2004 Elsevier B.V. All rights reserved.
doi:10.1016/j.margeo.2004.11.007

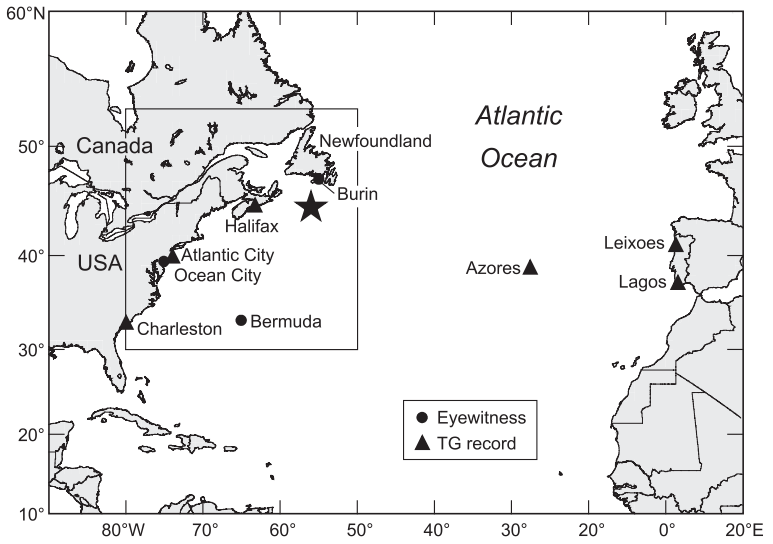

Fig. 1. Map of the North Atlantic Ocean showing the location of the 1929 Grand Banks earthquake epicenter (star) and the sites where the 1929 tsunami was recorded or seen by eye-witnesses.

earthquake was located at 44°30′ N, 57°15′ W (Fig. 1). The earthquake was felt as far away as New York City and Montreal but caused no damage because of its remoteness (Clague, 2001). However, the earthquake was accompanied by a tsunami (known as the "Grand Banks tsunami"), which was the most catastrophic tsunami in Canadian history: at least 27 people were killed in Newfoundland and 1 in Nova Scotia (Cranford, 2000; Clague et al., 2003). The tsunami was observed along the Atlantic coast of Canada and USA; the maximum waves occurred on the coast of Burin Inlet and the southeastern coast of Newfoundland (Fig. 1; Ruffman, 1997). Murty and Wigen (1976) studied the 1929 Grand Banks tsunami in detail and proposed that the significant amplification of waves arriving in Burin Inlet was associated with strong resonance in this V-shaped bay. The waves also crossed the Atlantic Ocean and were recorded on the coast of Portugal and at the Azores Islands (Clague, 2001).

Most submarine telegraph cables from North America to Europe at the time passed south of Newfoundland. An orderly sequence of breaks occurred in these cables following the Grand Banks earthquake at distances up to 500 km from the epicenter. According to Heezen and Ewing (1952), while all cables along the continental slope and rise south of the epicenter were broken, none of the continental shelf cables were disturbed. Heezen and Ewing (1952) and Heezen et al. (1954) presented evidence that the successive series of breaks in the telegraph cables (12 cables altogether) was caused by the turbidity current generated by the slump on the continental slope. Ultimately, the landslide was transformed into a turbidity current carrying mud and sand that flowed eastward up to 1000 km along the Atlantic floor onto the Sohm Abyssal Plain at speeds ranging from 60–100 km/h (Kuenen, 1952; Evans, 2001). The turbidity current had an estimated flow thickness of several hundred meters and must have flowed for at least 4 h and, more probably, about 11 h (Piper et al., 1988, 1999).

The area of the submarine failure coincided with the location of the earthquake epicenter. The subsequent ocean-floor mapping and the timing of the cable breaks on November 18, 1929 defined a zone of the earthquake-triggered slope failure of approximately 20,000 km^2 on the upper part of the continental slope. Further studies are in progress to better define this region and the prefailure distribution of sediment thicknesses (D.J. Piper, personal communication, 2003). The initial landslide involved Holocene and Pleistocene muds that moved downslope entraining coarser sediments. It is estimated that about 200 km^3 of material was displaced in the submarine landslide, a volume over 500 times greater than that of Canada's

largest known 1894 Saint-Alban subaerial slide (Piper et al., 1988, 1999; Evans, 2001).

Analyses of the 1929 Grand Banks tsunami indicate that it was generated by the large slope failure rather than by the earthquake itself (Murty, 1977; Clague, 2001). According to estimates made at the time of the disaster, tsunami heights ranged from 9 to 15 m along the coast of the Burin Peninsula, Newfoundland (Johnstone, 1930). However, recent field investigations suggest lower values: about 4.6 m in Burin and Port au Bras, 3 m in Lamaline and Point au Gaul, and 7.5 m in Taylor Bay (Ruffman, 1997; Clague et al., 2003). Horizontal runup distances were of the order of a kilometer in this area (Ruffman, 1997). Property damage, including the repair of the submarine cables, was $400,000 (in 1929 dollars); severe damage was exacerbated by the coincidence of the maximum tsunami waves with a peak tide (Clague et al., 2003).

The 1929 event gave rise to intense scientific and public interest. First, this was one of very few catastrophic tsunamis in the Atlantic occurring during the last 100 years (and probably the most destructive). Secondly, the tsunami had what was believed to be an uncommon generation mechanism: it was induced not directly by a seismic source but by a resultant submarine slope failure. Thirdly, this was one of very few slide-generated teletsunamis, recorded on the opposite side of the ocean far from the source area. Despite these considerations, no attempts have been made to simulate this tsunami due to the complexity of the source and problems with constructing a realistic three-dimensional numerical model of such landslide-generated tsunamis in a real ocean with highly complex bathymetry.

Recent catastrophic events (Indonesia, 1992; Skagway, 1994; Papua New Guinea, 1998; and Turkey, 1999) have greatly enhanced interest in landslide-generated tsunamis and promoted significant progress in their modeling. Encouraging results achieved over the past few years in numerical modeling of actual events (cf. Heinrich et al., 1998, 2000; Assier-Rzadkiewicz et al., 2000; Imamura et al., 2001; Thomson et al., 2001; Titov and González, 2001; Satake and Tanioka, 2003) prompted us to attempt to model the 1929 Grand Banks tsunami. Some preliminary results of this modeling are presented in this paper. Further refinements will follow as geological and geophysical investigations are completed; in particular, anticipated improvements in our understanding of such aspects as the precise landslide source area, sediment thicknesses, and initial failure styles will provide important inputs to a revised tsunami propagation model.

2. Governing equations and model description

The main difference between the 1929 Grand Banks submarine landslide and several other events, which have recently been examined, is the broad spatial size and large volume of this landslide. For example, the 1979 Nice failure (Mediterranean Sea) had an estimated volume of between $8.7 \cdot 10^{-3}$ and $70 \cdot 10^{-3}$ km^3 (Assier-Rzadkiewicz et al., 2000); the 1997 debris avalanche in Montserrat, Lesser Antilles had a volume of $40 \cdot 10^{-3}$ km^3 (Heinrich et al., 1998); the 1994 Skagway failure had, by different estimates, from $0.8 \cdot 10^{-3}$ (Kulikov et al., 1996; Rabinovich et al., 1999; Thomson et al., 2001) to $16.4 \cdot 10^{-3}$ km^3 (Mader, 1997; Kowalik, 1997). Thus, all these slides had volumes much less than 1 km^3. The massive underwater landslide associated with the 1998 PNG earthquake, which produced a catastrophic tsunami killing more than 2200 people, had a slide-body volume between 1 (Titov and González, 2001) and 4 km^3 (Heinrich et al., 2000). In contrast, the total sediment transport related to the 1929 Grand Banks slump was approximately 100–150 km^3 (Piper et al., 1988, 1999). The massive volume of this slide was ultimately responsible for the destructive consequences and widespread influence of the associated tsunami.

To simulate the 1929 tsunami, we divided the computational area into three domains:

(1) Internal domain (see inset in Figs. 2 and 3). This includes a rectangular area (41.6°N–46.0°N; 53.0°W–58.0°W) and covers a 151×184 grid with uniform grid steps $\Delta x = \Delta y = 2.67$ km.
(2) External domain (Fig. 2). This occupies a geographical area (30.0°N–53.0°N; 50.0°W–80.0°W) and includes a 901×938 grid with uniform grid steps; in Mercator projection $\Delta x = \Delta y = 2.0'$, which for longitude=2.67 km at 44°N.

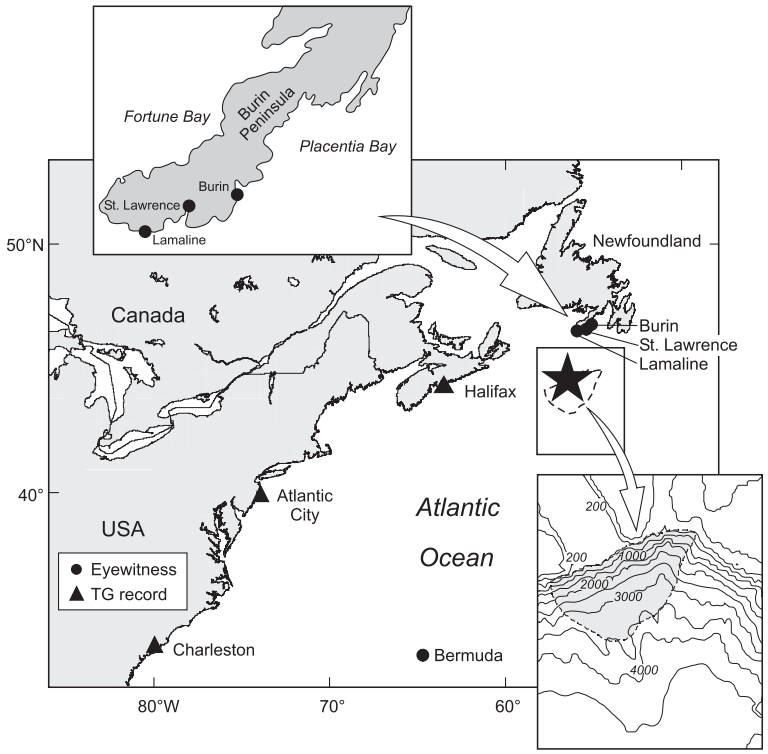

Fig. 2. The "external" computational domain, which was used for the 1929 tsunami simulation. The earthquake epicenter (star) and the observation sites are indicated. The inset in the bottom right corner shows the "internal" computational domain; shaded region denotes the area of the slide and the failure war directed downslope (southeastward). The inset in the upper left corner shows the area of the Burin Peninsula, southern Newfoundland, where maximum tsunami runup was observed.

(3) North Atlantic Ocean (Fig. 1). This occupies the entire basin of the North Atlantic Ocean between the equator and 70.0°N, and 80.0°W and 20.0°E, and covers a 1500×1585 grid with uniform grid steps in Mercator projection $\Delta x=\Delta y=4.0'$.

The first domain was used to simulate the slide motion and resultant tsunami waves generated by this motion; the second was applied to estimate tsunami wave heights in the vicinity of the source (Newfoundland coast) and along the eastern coast of North America; the third was used to calculate tsunami arrival times at various sites around the North Atlantic.

To simulate the 1929 tsunami, we used a modified viscous shallow-water model (Fine et al., 1998; Thomson et al., 2001; Rabinovich et al., 2003). The slide was assumed to be a viscous, incompressible fluid layer; water was taken to be inviscid and incompressible. We applied Mercator coordinates x, y, z, with z positive upward, x directed eastward, and y directed northward. Because of the relatively small area of the slide movement (~5°–6° in latitude), we used a simple plane projection for the slide modeling (i.e., for the internal domain); for larger areas (the external domain and North Atlantic domain), projection becomes important, and we made use of the more accurate Mercator equations for both long wave propagation and tsunami arrival time estimation.

The upper layer consists of seawater with density ρ_1, surface elevation $\eta(x,y;t)$, and horizontal velocity $\mathbf{u}$ with x, y components u, v; t is time. The lower layer consists of sediments of density ρ_2, kinematic viscosity ν, and horizontal velocity $\mathbf{U}$ with components U and V. Both the slope and the slide have low slopes, so that the motion is essentially horizontal. The slide is bounded by an upper surface $z=-h(x,y;t)$, the seabed is designated by $z=-h_s(x,y)$, and the thickness of the slide is $D(x,y;t)=h_s(x,y)-h(x,y;t)$. Quadratic friction

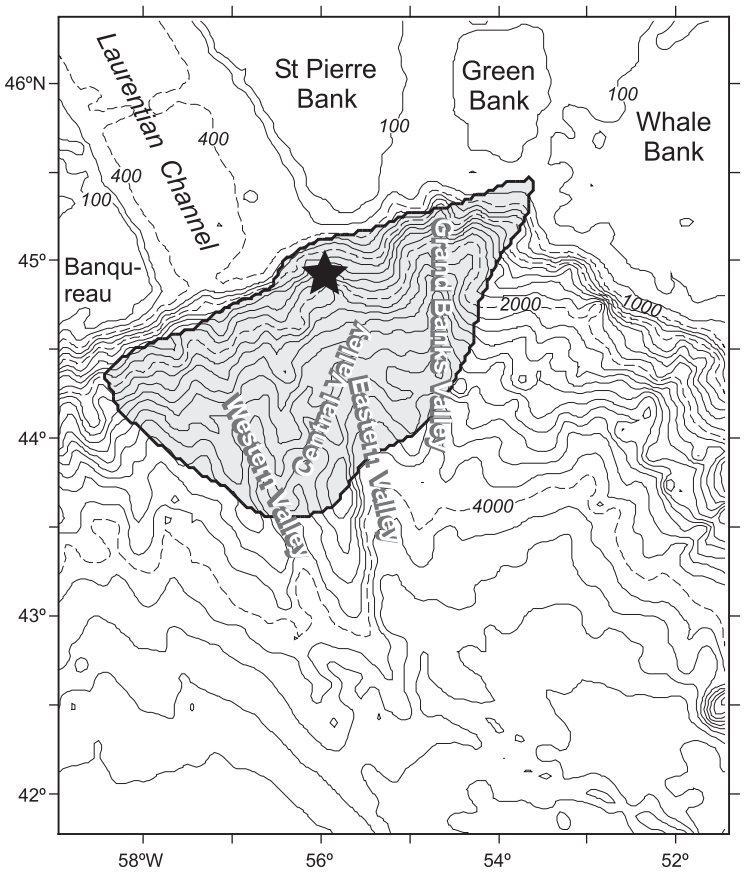

Fig. 3. Bathymetry of the Laurentian Fan with the location of the 1929 Grand Banks earthquake (marked by a star) and source area of the associated landslide.

is applied. Following Jiang and LeBlond (1994), we assumed that the density difference between flowslide and seawater is high, with $(\rho_2-\rho_1)\geq 0.2\ \mathrm{g\cdot cm^{-3}}$. In addition, we neglected the wave effect on the slide movement (so-called 'one-way coupled model'). As shown by Jiang and LeBlond (1992), this effect does not exceed 10%; for relatively deep-water slide movements, it is even less important. This approach allows us to divide the initial problem into two separate steps: (a) calculation of the slide motion to obtain the function $D(x,y;t)$; and (b) estimation of tsunami waves generated by the moving slide, using $D(x,y;t)$ as the source of the waves.

The main reason for using the viscous model and applying these assumptions is that field investigations and offshore geotechnical and geomorphological research showed that the 1929 failure on the Grand Banks slope was primarily a liquefaction flow (Piper et al., 1988, 1999). The physical background of the applied assumptions is thoroughly discussed by Jiang and LeBlond (1994) (see also Thomson et al., 2001; Rabinovich et al., 2003). At the seabed, the tangential velocity of the slide is set to zero, while at the upper surface of the slide, the vertical gradient in tangential velocity is set to zero. At steady state, horizontal velocities in the slide will then have a parabolic profile (Jiang and LeBlond, 1994):

$$\mathbf{U}(x,y,z,t)=\frac{3}{2}\mathbf{U}_{\mathrm{A}}(x,y,t)\left(2\xi-\xi^2\right), \tag{1}$$

where $\mathbf{U}_{\mathrm{A}}$ is the vertically averaged horizontal slide velocity, and

$$\xi=(z+h_{\mathrm{s}})/D \tag{2}$$

is a normalized depth. Conservation of mass and momentum for a viscous slide have the form (Fine et al., 1998):

$$\frac{\partial D}{\partial t} + \left(\vec{\nabla} \cdot D\mathbf{U}_\mathrm{A}\right) = 0; \tag{3}$$

$$\frac{1}{D}\frac{\partial D\mathbf{U}_\mathrm{A}}{\partial t} + \frac{6}{5}\frac{1}{D}\left(\mathbf{U}_\mathrm{A}\cdot\vec{\nabla}\right)D\mathbf{U}_\mathrm{A} = -g\frac{\rho_2-\rho_1}{\rho_2}\vec{\nabla}\left(D-h_\mathrm{s}\right) - \frac{2\nu\mathbf{U}_\mathrm{A}}{D^2} - \frac{c\mathbf{U}_\mathrm{A}|\mathbf{U}_\mathrm{A}|}{D}, \tag{4}$$

where the feedback effect of the wave on the slide movement is neglected on the right side of the momentum Eq. (4). The last term in Eq. (4) was added to include the quadratic friction, caused by drag effects at high slide speeds. The boundary conditions include that of no slide transport through the coastal boundary, G, and the assumption that the slide does not cross the outer (open) boundary, Γ. No "stop condition" was applied to the downslope slide motion. Instead, we consider this slide motion only for a limited time; after this time, we only simulate freely propagating tsunami waves. It is important to emphasize that our purpose is not to simulate the entire motion and transformation of the Grand Banks slide and associated turbidity flow (propagating over 500 km), but to consider only the initial stage of the event responsible for the generation of the tsunami waves.

The upper (water) layer of the model is governed by the linear shallow water equations (in Mercator projection):

$$\frac{\partial\eta}{\partial t} + \frac{\cos\varphi_0}{\cos\varphi}\left[\frac{\partial(hu)}{\partial x} + \frac{1}{\cos\varphi}\frac{\partial(hv\cos\varphi)}{\partial y}\right] = \frac{\partial D}{\partial t}; \tag{5}$$

$$\frac{\partial\mathbf{u}}{\partial t} = -\frac{\cos\varphi_0}{\cos\varphi}g\vec{\nabla}\eta, \tag{6}$$

where φ and φ_0 are the current and the reference latitudes. In effect, the slide generates water waves through the continuity Eq. (5) only. The waves then propagate within the restrictions imposed by the boundary conditions and the momentum Eq. (6). At the open boundary, Γ, we use the one-dimensional radiation condition for outgoing waves:

$$u_\mathrm{n} = \eta\sqrt{\frac{g}{h}}, \tag{7}$$

where u_n is the velocity component normal to Γ. At the shore, G, we assume a vertical wall, so that

$$u_\mathrm{n} = 0 \text{ at } G. \tag{8}$$

An explicit finite-difference method was used to solve Eqs. (3)–(4) for the viscous slide and Eqs. (5)–(6) for the waves, with boundary conditions (7) and (8). To avoid generation of erroneous small-scale oscillations, the time step (Δt) was chosen to be 1/3 of the value required for the Courant–Friedrich–Levy (CFL) stability criterion. Since the slide is initially at rest, all velocity components and the sea surface elevation are set to zero at t=0. Detailed verification of this model was carried out by Rabinovich et al. (2003). A similar viscous slide long-wave model was also used by others to examine the 1994 Skagway tsunami (Rabinovich et al., 1999; Thomson et al., 2001), the 1999 Papua New Guinea tsunami (Heinrich et al., 2000; Titov and González, 2001; Imamura et al., 2001), and the 1979 Nice harbour slide-generated tsunami (Assier-Rzadkiewicz et al., 2000). In all cases, the model produced reasonable agreement with observations.

2.1. Slide and tsunami modeling

In the first stage of our simulation of the 1929 slide and tsunami, we used the internal domain (Fig. 2, inset). Parameters of the landslide have been chosen according to geotechnical and morphological preliminary estimates (Piper et al., 1988, 1999):

Initial slide area: 20,000 km^2;
Volume: 125 km^3 ;
Thickness: 5 m;
Sediment density (ρ_2): 2.0 g·cm^{-3};
Kinematic viscosity (ν): 0.01 m^2·s^{-1};
Drag coefficient: 0.0025;
Slide motion time: 3000 s.

In the first model runs, we treated the slide as a body with uniform thickness of 5 m; clearly, this is an

oversimplification, which will be improved upon in later refinements of the model as more geological results are forthcoming. We assumed that all movement started simultaneously over the entire 20,000 km^2 area. Of course, these assumptions are valid for rough estimation purposes only and need to be corrected with more sophisticated models of the initial failure.

In contrast to rigid slides, which move as single consolidated bodies, preserving their size and form, viscous slides normally spread and flatten as they move downslope. The significant area of the Grand Banks slide and the complicated topography in the source region resulted in several separate failures. These mud flows merged in submarine canyons, located in and southward from the source area (Fig. 3), and moved downslope along the thalweg lines. The concentrated and focused moving slide mass (similar to snow/ice avalanches in mountains) was apparently the main reason for the numerous cable breaks. The resultant modeled slide speed (controlled by quadratic friction) was about 100 km/h, in close agreement with the observations.

Fig. 4 presents snapshots of the simulated slide movement for times t=10, 20, 30, and 40 min. These snapshots demonstrate the prominent difference of the 1929 Grand Banks slide from other slides that we have previously simulated, in particular, the 1994 Skagway dock failure slide (Rabinovich et al., 1999; Thomson et al., 2001) and hypothetical slides in Malaspina Strait and in the southern part of the Strait of Georgia (Rabinovich et al., 2003). In these previous cases, the moving slide bodies had pronounced arcuate shapes, which is a typical feature of moving viscous fluid slides (Jiang and LeBlond, 1994). In contrast, the 1929 slide mainly moved along steep Western, Central, Eastern, and Grand Banks submarine valleys shown in Fig. 3, forming peculiar slide "tongues" (20, 30, and 40 min in Fig. 4). Recent Seabeam, SeaMARC 1, and Système Acoustique Remorqué (SAR) high-resolution sonar and seismic profiles made on the St. Pierre Slope showed till tongues extending to water depths of 500 m (Piper et al., 1988, 1999; Huges Clarke et al., 1990). The detailed ocean floor mapping indicated that, below approximately 4000 m, these multiple slide flows merged into two main debris flows leading along two main valleys (Eastern and Western) that extended to

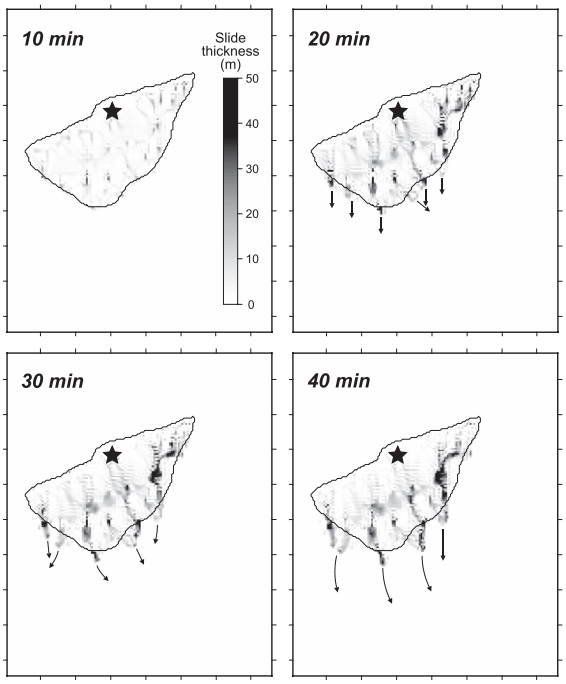

Fig. 4. Snapshots of simulated slide flows for 10, 20, 30, and 40 min after the initial 1929 Grand Banks slide failure. The star indicates the epicenter of the earthquake; arrows show the directions of slide flow.

water depths of about 5000 m, where they debouched onto the Sohm Abyssal Plain (Piper et al., 1988). However, we did not try to simulate these deep-ocean slide motions, which play a negligible role in formation of tsunami waves, and limited our consideration of the slide to the first 50 min.

The principal result of our computation is the simulated slide function $D(x,y;t)$, describing the first 50 min of the slide movement and the evolution of the slide body. In the second stage of our computations, this function was used as the source for the generated surface waves. For the latter computations, we applied the external domain (Fig. 2). Fig. 5 presents snapshots of simulated tsunami waves at various times following failure. The slide movement was mainly directed southward and southeastward, spreading cylindrical surface waves ahead of it. Local topography near the source area and the general orientation of the east coast of North America determine the specific sector-like form of the propagating frontal wave. At the same time, due to wave reflection from the shelf of

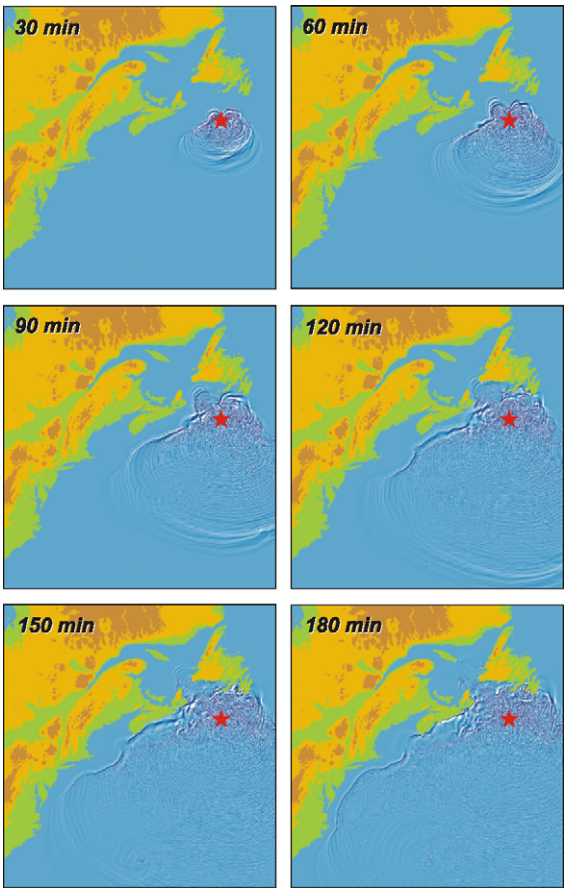

Fig. 5. Snapshots of simulated tsunami waves for 30, 60, 90, 120, 150, and 180 min after the 1929 Grand Banks slide failure. The star indicates the epicenter of the earthquake.

Newfoundland and Nova Scotia, the tsunami waves form a complicated structure of standing oscillations near the source area. Strong resonant effects, occurring in some straits and inlets of the Newfoundland coast, probably explain the catastrophic tsunami runup observed in this region.

Several other observations can be made concerning the propagation of tsunami waves from the source (marked by the star in Fig. 5):

(1) the waves propagate rapidly northwestward through the deeper Laurentian Channel toward Anticosti Island;
(2) there is an observable interaction between the tsunami waves and the New England Seamounts, a lineation of features extending southeastwards from approximately Cape Cod; and,
(3) tsunami waves become "trapped" by Bermuda as they refract around the islands.

Fig. 6 shows simulated wave records (surface sea level elevations) at St. Lawrence, Burin, Lamaline (all located on the coast of the Burin Peninsula, the southernmost part of Newfoundland Island), Halifax (Nova Scotia), Atlantic City (New Jersey), and Bermuda (see locations of these sites in Figs. 1 and 2). Burin Peninsula (see inset in Fig. 2) was the region of the largest 1929 tsunami runup and accounted for almost all of the casualties (cf. Murty and Wigen, 1976; Ruffman, 1997; Cranford, 2000). Another area of significant tsunami waves was the eastern coast of Nova Scotia. Results of computations qualitatively agree with the observations: maximum simulated wave heights are for the coast of Burin Peninsula and Nova Scotia (albeit, computed wave heights are

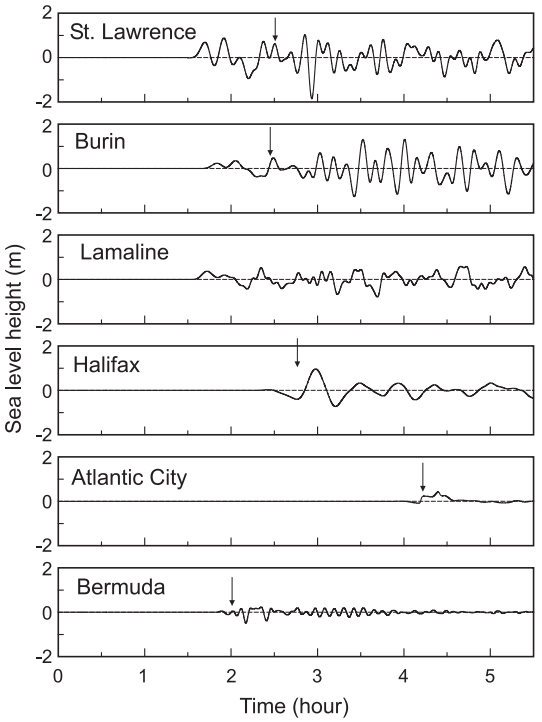

Fig. 6. Simulated tsunami records at St. Lawrence, Burin, Lamaline (all on the Burin Peninsula, Newfoundland), Halifax (Nova Scotia), Atlantic City (New Jersey), and Bermuda. Arrows indicate observed tsunami arrival times.

considerably smaller than those observed). At the same time, model results reproduce some features of the wave behavior at various sites (Fig. 6) which are probably important for understanding the generation mechanism of the catastrophic waves. Significant differences in Q-factor and wave periods indicate that the topography, rather than the source, determines wave properties of tsunami waves in this region. Long "ringing" and slow energy decay are essential properties of the oscillations on the coast of Burin. Apparently, as was assumed by Murty and Wigen (1976), oscillations observed at these sites were associated with strong resonance in Burin Inlet. Typical periods of simulated waves are 12–15 min in St. Lawrence and Burin, and about 25 min in Lamaline. It is quite difficult to select the highest wave because the waves display approximately the same height over a long period of time, consistent with strong resonant effects and a high Q-factor for the inlet.

Simulated tsunami waves in Halifax and Atlantic City were significantly different from those for the Burin coast. The frontal wave was the highest, and then the energy of the oscillations decayed rapidly. The period of the simulated tsunamis in Halifax was about 40 min. Interesting behavior of the simulated waves is observed for Bermuda. During the first hour, the oscillations were erratic; however, they then became very regular with period of about 10 min (Fig. 6). Apparently, as mentioned above (see Fig. 5), the waves became trapped around the islands.

2.2. Observations

Berninghausen (1968) noted that the 1929 Grand Banks tsunami was observed at over 30 locations on the coast Newfoundland, including the Saint-Pierre and Miquelon Islands, the eastern coasts of Canada and USA, and the Bermuda Islands. It was also recorded in the Azores Islands and Portugal (Lander and Lockridge, 1989; Ruffman, 1997). The high amplitude and widespread extent of this tsunami prompted us to consider whether the tsunami might also have been observed at coastal sites on the eastern side of the Atlantic.

Wigen (1989) made a significant effort to locate tsunami records and to find other information on this tsunami. He received replies from Iceland, Norway, the United Kingdom, Spain, and France, informing him that through wartime damage and other causes, no records appeared to exist. Hourly wave heights still remained for several sites; however, they showed no evidence of the tsunami. A tide station was reported to have been operated at that time in Bermuda, but William Donn, Coordinator of the Atmospheric Science Programs, in December 1973 was unable to locate the records.

Wigen (1989) reported that he had received analogue tide gauge records for Ponta Delgada, Azores Islands (from Sevico Meteorologico Nacional, Portugal) and Leixoes, northern Portugal (from Geomarine Associates; see locations in Fig. 1). The tsunami arrived at the Azores at 0055 GMT (travel time of 4 h 23 m) and at Leixoes at 0250 GMT, November 19, 1929 (travel time of 6 h 18 m). Unfortunately, maregrams for Madeira Islands, Portuguese Guinea, Cape Verde, and Angola for that period were destroyed in a fire in 1969 in the Hydrographic Institute in Lisbon.

The US tide gauge diagrams obtained by Geomarine Associates for Eastport (Maine), Portland (Maine), Boston (Massachusetts), and Key West (Florida) indicated no tsunami. In contrast, the Atlantic City (New Jersey) diagram showed a clear tsunami record that commenced at 0045 GMT with a sudden rise of 26 cm, continued rising to a maximum of 68 cm at 0424 GMT, and then gradually diminished. Also, the Charleston (South Carolina) tide gauge recorded a single rise of 12 cm over a period of 30 min at 0220 GMT, with subsequent return to normal sea level (Wigen, 1989). In addition, Lander and Lockridge (1989) report waves at Bar Harbour, Belfast, and Portland (Maine), Barnstable (Massachusetts), and Block Island (Rhode Island). They also credit Berninghausen (1968) regarding an about 0.3-m wave at Ocean City (Maryland).

Unfortunately, all our attempts to find all these records proved difficult. Fig. 7 presents the only quality record (Halifax, Nova Scotia), which we could readily locate in Wigen's archive. The observed wave height of the first crest wave is about 60 cm, and the period of the first wave is about 40 min. These results are in good agreement with our numerical computations for this site (Fig. 6). The

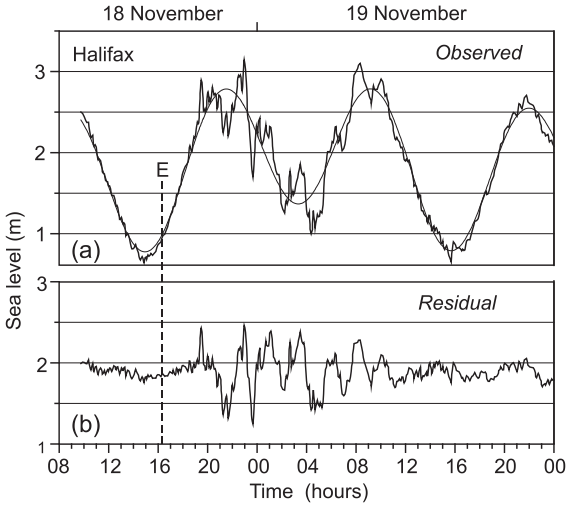

Fig. 7. Observed 1929 tsunami record at Halifax: (a) original and (b) residual (detided).

ensuing oscillations, however, had a significantly longer period (a few hours), with the total duration of the train about 20 h. We infer that these oscillations were formed by tsunami-induced trapped edge waves propagating along the continental shelf. The clearly dispersive character of the observed waves (the observed period decreased from 4 to 2.5 h) supports this conclusion. Beardsley et al. (1977) observed on the continental shelf of the Middle-Atlantic Bight (located south of Nova Scotia) a similar train of dispersive first-mode edge waves with periods 5–7 h generated by a sudden pressure drop. The short duration of the simulated records (about 6 h, see Fig. 6) and insufficient topographic resolution has not allowed us to examine this type of wave in the present study.

Dr. Pedro Miranda from the University of Lisbon kindly provided us with a record for Lagos, Portugal (see Fig. 1), showing tsunami oscillations measured at this site on November 19, 1929. The observed period of these oscillations was about 20–25 min. This record as well as the reported records for Azores Islands and Leixoes (Wigen, 1989) clearly demonstrate that the 1929 tsunami crossed the Atlantic and was observed on the opposite coast. Unfortunately, the beginning of the 1929 Lagos record is missing, and the quality of the record is poor. It is noteworthy that the Portugal stations (Lagos, Leixoes, and Azores) also recorded two other significant tsunamis in the Atlantic; in 1969 and 1975 (Rabinovich et al., 1998).

2.3. Tsunami travel times

Berninghausen (1968) used over 30 locations in Newfoundland, Nova Scotia, the east coast of the US, and Bermuda, where the 1929 tsunami was seen visually or recorded by tide gauges, to draw an empirical tsunami travel time map and estimate arrival times of tsunami waves at various sites. We used this information, slightly corrected by the information in Wigen (1989), to produce Table 1 ("Observed") and Fig. 7 (indicated by arrows). We estimated the same time theoretically using the results of our numerical model ("Computed" in Table 1). We also used the "North Atlantic domain" to construct the tsunami travel map for the entire North Atlantic (Fig. 8) and calculate tsunami arrival times along the eastern Atlantic coast. In most cases, the observed and computed arrival times are quite good agreement. The only region of noticeable disagreement is the Burin Peninsula: computed arrival times for this region are 35–50 min smaller than the observed (observed arrival time for St. Lawrence is taken from Ruffman, 1997). Future improvements in the model will be focused specifically on this region.

Tsunami travel times demonstrate the strong anisotropy of the propagating waves (clearly seen in Fig. 8). The waves reach open ocean islands such as Bermuda in about 2 h (mean speed ~700 km/h) and the Azores in about 4 h (~630 km/h). At the same time, tsunami wave speeds are much slower in the

Table 1
Travel times of the 1929 Grand Banks tsunami from the source area to various sites

Location	Approximate distance (km)	Arrival time	
		Observed	Computed
Burin, Newfoundland	340	2 h 23 m	1 h 48 m
Halifax, NS	610	2 h 46 m	2 h 35 m
Bermuda Islands	1445	2 h 00 m	1 h 50 m
Atlantic City, NJ	1630	4 h 13 m	4 h 13 m
Ocean City, MD	1700	3 h 48 m	4 h 05 m
Charleston, NC	2450	5 h 48 m	5 h 20 m
Azores, Portugal	2440	4 h 23 m	3 h 55 m
Leixoes, Portugal	3980	6 h 18 m	6 h 30 m
Lagos, Portugal	4060	?	6 h 47 m

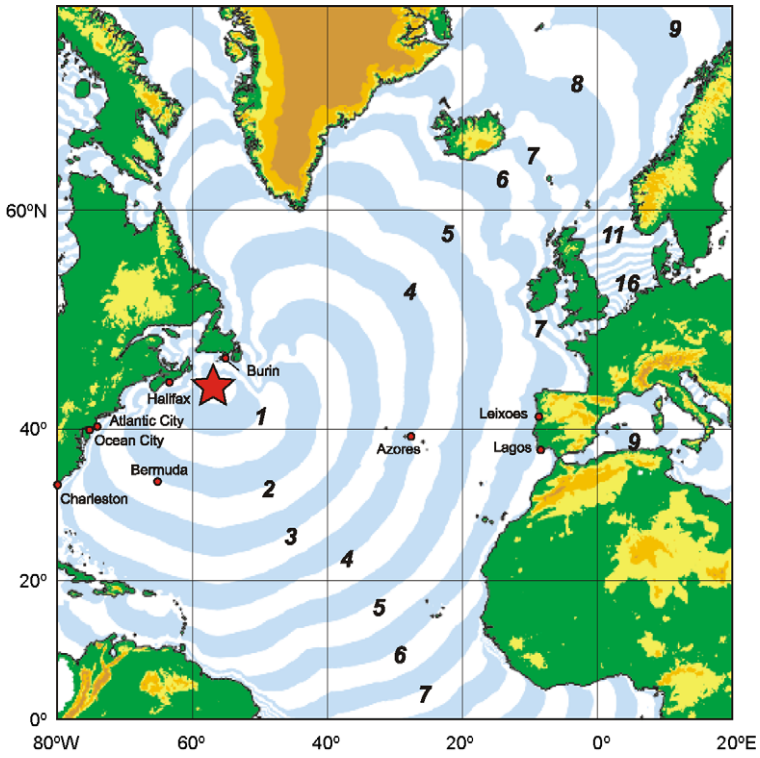

Fig. 8. Map of the estimated tsunami travel times (in hours) in the North Atlantic Ocean for waves generated by the 1929 Grand Banks slide failure. Red circles indicate the observation sites (see Table 1).

direction of the North American coast: they require 2.7 h to reach Halifax (~230 km/h) and 4.2 h to reach Atlantic City (~380 km/h).

3. Discussion

In general, tsunami waves can be generated by an underwater landslide through two different mechanisms. First is a piston-like effect: the moving underwater slide pushes water upward and laterally above the frontal part of the slide and draws it downward at the rear of the failure. Similar thrust-like effects are believed to be the major mechanism for earthquake-generated tsunamis. Seismically related seafloor motions have time scales much shorter than the typical time of wave propagation, which is why the initial sea level elevation can usually be taken as equal to the residual sea-floor displacement. In the case of a landslide-generated tsunami, the time scale for both the wave motion and slide motion is comparable. The efficiency of the generation depends on the slide-thickness/depth ratio, such that the initial slide movement, occurring before the slide leaves the shallow-water area, is crucial in terms of tsunami generation. For this reason, the initial position of the slide and distribution of the slide thickness as well as the timing of the failure play key roles in the formation of maximum tsunami wave heights. Unfortunately, the current lack of precise data on the slide body leads us to use a very rough model of uniform thickness. It is clear that, in reality, large unstable sediment masses, which are mainly associated with alluvial deposits from the St. Lawrence River, are accumulated in submarine canyons and valleys and are not distributed uniformly over the source area. It is important to emphasize that progress in understanding the 1929 event, and in achieving better agreement with the observational data on the coast of Burin Peninsula (i.e., the area where the actual tsunami runup was more than

10 m and the most casualties occurred), is apparently related more to a better knowledge of the parameters of the initial slide failure and to the availability of more precise seafloor topography than to improvements in the numerical model itself (e.g., using the Navier–Stokes or Boussinesq equations instead of the shallow-water equations). In fact, the same can be said of many slide-generated tsunamis occurring in other regions of the world ocean.

Another effect that may be important for the 1929 event is the nonpiston-like interaction between the water and the slide. This is the second mechanism to generate slide-related tsunami waves. With an increase in slide velocity, the slide is transformed into a turbidity current with high mass and momentum exchange with the surrounding seawater. A simple estimation shows that the impulse transfer of energy into the water is significant. The mechanics of this impulse transfer through water column is unclear at present, although for the 1929 event (which is known to be accompanied by a destructive turbidity flow), it may be important.

4. Conclusions

Our model provides a successful initial simulation of the tsunami resulting from the 1929 earthquake-generated sediment failure on the continental slope off southern Newfoundland. The failure was modeled as a flow slide whose motion was controlled by the actual seafloor morphology in the region. Our results are encouraging in that the arrival times—and to a lesser degree, the amplitudes—of the tsunami waves at various control sites is in reasonable agreement with visual observations and tide gauge records.

This work is preliminary in nature and was meant to formulate the problem and attempt to provide some preliminary model estimates. We will be refining the results based on ongoing geological, geophysical, and geotechnical studies; in particular, we shall incorporate better estimates of initial position, failure thicknesses, volumes, and physical properties as they become available. Further tide gauge records and other observational data will be sought in order to verify and tune the model in terms of arrival times and amplitudes. Sensitivity analyses will be undertaken to test the effects of altering important parameters such as density, viscosity, failure styles, volumes, and slide distribution. If possible, the inverse tsunami problem will be attempted in which tsunami observed properties (e.g., travel times, amplitudes) will be used to constrain the failure–tsunami model.

Acknowledgments

This research was in large part sponsored by Natural Sciences and Engineering Research Council of Canada (COSTA-Canada). We wish to thank Dr. Pedro Miranda (University of Lisbon, Portugal) for information on the manifestation of the 1929 tsunami on the coast of Portugal. Dr. David Piper provided important information on the slide source area and failure styles. Discussions with several other members of the COSTA-Canada team, in particular its principal investigator Jacques Locat, added considerably to the progress of the modeling. Patricia Kimber drafted the figures.

References

Assier-Rzadkiewicz, S., Heinrich, P., Sabatier, P.C., Savoye, B., Bourillet, J.F., 2000. Numerical modelling of landslide-generated tsunami: the 1979 Nice event. Pure Appl. Geophys. 157, 1707–1727.

Beardsley, R.C., Mofjeld, H., Wimbush, M., Flagg, C.N., Vermersch Jr., J.A., 1977. Ocean tides and weather-induced bottom pressure fluctuations in the Middle-Atlantic Bight. J. Geophys. Res. 82 (21), 3175–3182.

Berninghausen, W.H., 1968. Tsunamis and seismic seiches reported from the western North and South Atlantic and the coastal waters of Northwestern Europe. U.S. Naval Oceanographic Office, Geology Section, Marine Environmental Branch, Oceanographic Analysis Division. Informal Report IR #68-85, 48 p.

Clague, J.J., 2001. Tsunamis. In: Brooks, G.R. (Ed.), A Synthesis of Geological Hazards in Canada, Geological Survey of Canada Bull. 548, 27–42.

Clague, J.J., Munro, A., Murty, T.S., 2003. Tsunami hazard and risk in Canada. Nat. Hazards 28, 433–461.

Cranford, G., 2000. Tidal Wave. A List of Victims and Survivors, Newfoundland, 1929. Flanker Press, St. John's, Newfoundland. 264 pp.

Evans, S.G., 2001. Landslides. In: Brooks, G.R. (Ed.), A Synthesis of Geological Hazards in Canada, Geological Survey of Canada, Bull. 548, 43–79.

Fine, I.V., Rabinovich, A.B., Kulikov, E.A., Thomson, R.E., Bornhold, B.D., 1998. Numerical modelling of landslide-generated tsunamis with application to the Skagway Harbor

tsunami of November 3, 1994. Proceedings, International Conference on Tsunamis, Paris, pp. 211–223.
Heezen, B.C., Ewing, M., 1952. Turbidity currents and submarine slumps and the 1929 Grand Banks earthquake. Am. J. Sci. 250, 849–873.
Heezen, B.C., Ericson, D.B., Ewing, M., 1954. Further evidence for turbidity current following the 1929 Grand Banks earthquake. Deep Sea Res. 1, 193–202.
Heinrich, P., Mangeney, A., Guibourg, S., Roche, R., Boudon, G., Vheminée, J.-L., 1998. Simulation of water waves generated by a potential debris avalanche in Montserrat, Lesser Antilles. Geophys. Res. Lett. 25 (19), 3697–3700.
Heinrich, P., Piatensi, A., Okal, E., Hébert, H., 2000. Near-field modeling of the July 17, 1998 tsunami in Papua New Guinea. Geophys. Res. Lett. 27, 3037–3040.
Huges Clarke, J.E., Shor, A.N., Piper, D.J.W., Mayer, L.A., 1990. Large-scale current-induced erosion and deposition in the path of the 1929 Grand Banks turbidity current. Sedimentology 37, 613–629.
Imamura, F., Hashi, K., Imteaz, Md.M.A., 2001. Modeling for tsunamis generated by landsliding and debris flow. In: Hebenstreit, G. (Ed.), Tsunami Research at the End of a Critical Decade. Kluwer, Dorderecht, pp. 209–228.
Jiang, L., LeBlond, P.H., 1992. The coupling of a submarine slide and the surface waves which it generates. J. Geophys. Res. 97 (C8), 12731–12744.
Jiang, L., LeBlond, P.H., 1994. Three-dimensional modeling of tsunami generation due to a submarine mudslide. J. Phys. Oceanogr. 24 (3), 559–572.
Johnstone, J.H.L., 1930. The Acadian–Newfoundland earthquake of November 18, 1929. Proc. Trans. N. S. Inst. Sci. 17, 223–237.
Kowalik, Z., 1997. Landslide-generated tsunami in Skagway, Alaska. Sci. Tsunami Hazards 15 (2), 89–106.
Kuenen, P.H., 1952. Estimated size of the Grand Banks turbidity current. Am. J. Sci. 250, 874–884.
Kulikov, E.A., Rabinovich, A.B., Thomson, R.E., Bornhold, B.D., 1996. The landslide tsunami of November 3, 1994, Skagway Harbor, Alaska. J. Geophys. Res. 101 (C3), 6609–6615.
Lander, J.F., Lockridge, P.A., 1989. United States Tsunamis, 1690 to 1988, Publ. 41–2. National Geophysical Data Center, Boulder, CO, 265 pp.
Mader, C.L., 1997. Modeling the 1994 Skagway tsunami. Sci. Tsunami Hazards 15 (1), 41–48.
Murty, T.S., 1977. Seismic sea waves–tsunamis. Bull. Fish. Res. Board Can. 198, 337 pp.
Murty, T.S., Wigen, S.O., 1976. Tsunami behavior on the Atlantic coast of Canada and some similarities to the Peru coast. Proc. IUGG Symp. Tsunamis and Tsunami Res., Jan. 29–Feb. 1, 1974, Wellington, N.Z. R. Soc. N. Z. Bull., 15, 51–60.
Piper, D.J.W., Shor, A.N., Hughes Clarke, J.E., 1988. In: Clifton, H.E. (Ed.), The 1929 "Grand Banks" Earthquake, Slump, and Turbidity Current, Spec. Pap.-Geol. Soc. Am. 229, 77–92.
Piper, D.J.W., Cochonat, P., Morrison, M.L., 1999. The sequence of events around the epicenter of the 1929 Grand Banks earthquake: initiation of debris flows and turbidity current inferred from sidescan sonar. Sedimentology 46, 79–97.
Rabinovich, A.B., Miranda, P., Baptista, M.A., 1998. Analysis of the 1969 and 1975 tsunamis at the Atlantic coast of Portugal and Spain. Oceanology 38 (4), 463–469.
Rabinovich, A.B., Thomson, R.E., Kulikov, E.A., Bornhold, B.D., Fine, I.V., 1999. The landslide-generated tsunami of November 3, 1994 in Skagway Harbor, Alaska: a case study. Geophys. Res. Lett. 26 (19), 3009–3012.
Rabinovich, A.B., Thomson, R.E., Bornhold, B.D., Fine, I.V., Kulikov, E.A., 2003. Numerical modelling of tsunamis generated by hypothetical landslides in the Strait of Georgia, British Columbia. Pure Appl. Geophys. 160 (7), 1273–1313.
Ruffman, A., 1997. Tsunami runup mapping as an emergency preparedness planning tool: the 1929 tsunami in St. Lawrence, Newfoundland. Geomarine Associates, Contract Report for Emergency Preparedness Canada (EPC), Ottawa, Ontario, Vol. 1, 107 pp.
Satake, S., Tanioka, Y., 2003. The July 1998 Papua New Guinea earthquake: mechanism and quantification of unusual tsunami generation. Pure Appl. Geophys. 160 (7), 2087–2118.
Thomson, R.E., Rabinovich, A.B., Kulikov, E.A., Fine, I.V., Bornhold, B.D., 2001. On numerical simulation of the landslide-generated tsunami of November 3, 1994 in Skagway Harbor, Alaska. In: Hebenstreit, G. (Ed.), Tsunami Research at the End of a Critical Decade. Kluwer, Dorderecht, pp. 243–282.
Titov, V., González, F., 2001. Numerical study of the source of the July 17, 1998 PNG tsunami. In: Hebenstreit, G. (Ed.), Tsunami Research at the End of a Critical Decade. Kluwer, Dorderecht, pp. 197–207.
Wigen, S.O., 1989. Report on the Assessment and Documentation of Tsunamis for Eastern Canada. Unpublished Manuscript. Tide and Tsunami Services, Fulford Harbour, B.C., 16 pp.